Plasma Physics and
Controlled Fusion

Neutron measurements at the KATANA water-activation loop using the neutron activation method

To cite this article: J Wlodarczyk *et al* 2026 *Plasma Phys. Control. Fusion* **68** 035003

Plasma Physics and Controlled Fusion

OPEN ACCESS

RECEIVED
21 November 2025

REVISED
4 February 2026

ACCEPTED FOR PUBLICATION
16 February 2026

PUBLISHED
27 February 2026

PAPER

Neutron measurements at the KATANA water-activation loop using the neutron activation method

J Wlodarczyk[1,*], B Bienkowska[1], E Laszynska[2], D Govekar[3,5], D Kotnik[3], I Lengar[3], X Litaudon[4], J Peric[3,5], V Radulovic[3,5], L Snoj[3,5] and R Villari[6]

[1] Institute of Plasma Physics and Laser Microfusion, Hery 23, 01-497 Warsaw, Poland
[2] Faculty of Energy and Fuels, Department of Nuclear Energy and Radiochemistry, AGH University of Krakow, al. A. Mickiewicza 30, 30-059 Krakow, Poland
[3] Reactor Physics Department, Jozef Stefan Institute, Jamova cesta 39, Ljubljana SI-1000, Slovenia
[4] CEA, F-13108 St-Paul-Lez-Durance, France
[5] Faculty of Mathematics and Physics, University of Ljubljana, Jadranska cesta 19, Ljubljana 1000, Slovenia
[6] NUC Department, ENEA, Via E. Fermi 45, 00044 Frascati, Rome, Italy
[*] Author to whom any correspondence should be addressed.

E-mail: jakub.wlodarczyk@ifpilm.pl

Keywords: neutron activation method, water activation experiments, KATANA, ITER, ^{17}N

Abstract

As the primary coolant, water is used in most current fission reactors and is also a promising coolant for future fusion devices. During normal operation, the fusion device produces plasma discharges. The primary cooling water circulates through in-vessel cooling channels and thus passes through regions of high neutron flux ($E \sim 14$ MeV) produced by D–T fusion. During this process, cooling water can be activated and produce radioactive nuclides that emit gamma rays and neutrons (neutron energy range 0.4–1.7 MeV). Predicting the dose-rate field—the spatial and temporal distribution of radiation dose rates ($\mathrm{Sv \cdot h^{-1}}$) produced by activated nuclides in the flowing coolant—requires coupling computational fluid dynamics (CFD) with radiation-transport and activation calculations. To validate these coupled CFD + radiation-transport + activation models and to investigate how production, transport and decay of activation products together create the observed dose-rate field, the KATANA water-activation loop at the Jožef Stefan Institute Training, Research, Isotope production, General Atomics Mark II reactor was commissioned. This paper examines the newly established KATANA water-activation loop and evaluates the feasibility of using the neutron activation method for neutron measurements at the facility. The studies show that this method can be successfully applied to detect and quantify neutrons originating from ^{17}N decay. Furthermore, the measurements demonstrate that this technique is capable of characterising the neutron emission rate at the KATANA water-activation loop. Finally, the paper proposes a method for estimating the neutron fluence at selected sample positions. The results encourage further use of the neutron activation method to investigate neutrons emitted by activated water. Future experiments could determine the neutron fluence-rate profile, thereby validating fluid-activation codes for ITER, DEMO and other fusion devices. This would also contribute to reducing the uncertainty of the $^{17}\mathrm{O}(n,p)^{17}\mathrm{N}$ reaction cross-section.

1. Introduction

Most fission reactors use light water as a coolant due to its affordability, widespread availability and high heat capacity. Light water is also expected to play a key role in future fusion reactors. It was already used as a cooling fluid in various operational systems at JET [1] and WEST [2], and it is planned for cooling the ITER [3] vacuum vessel and other auxiliary systems.

Water that cools in-vessel components is exposed to high-energy (~14 MeV) neutrons produced by deuterium–tritium (D–T) fusion. Since water consists of hydrogen and oxygen, both elements can be

Table 1. The most important water-activation reactions, including natural abundances of target nuclides, half-lives of the product nuclides, and information on emitted particles (their energies and intensities). Based on the ENDF/B-VIII.0 nuclear data library [7].

Reaction	Natural abundance	Half-life, $T_{1/2}$	Released particles
$^{16}O(n,p)^{16}N$	99.76%	7.13 s	γ: 6.129 MeV (67%) γ: 7.115 MeV (5%)
$^{17}O(n,p)^{17}N$	0.04%	4.17 s	***n***: 0.383 MeV (35%) γ: 0.871 MeV (3%) ***n***: 1.171 MeV (53%) ***n***: 1.700 MeV (7%)
$^{18}O(n,\gamma)^{19}O$	0.20%	26.88 s	γ: 0.110 MeV (3%) γ: 0.197 MeV (96%) γ: 1.357 MeV (50%) γ: 1.444 MeV (3%)

activated by neutrons. While hydrogen activation is often negligible [4], oxygen activation is significant; the principal activation products are ^{16}N, ^{17}N, and ^{19}O. Details on water-activation products are presented in table 1. The decay of ^{16}N and ^{19}O results primarily in gamma emission, whereas decay of ^{17}N produces gamma rays and emits neutrons with discrete energies of 0.383 MeV, 1.171 MeV and 1.700 MeV. These secondary particles warrant investigation as activated water circulates through the primary cooling loop and, in many cases, beyond the biological shield. During circulation the activated water decays, emitting neutrons and gamma rays that contribute to doses received by personnel and increase the radiation exposure of sensitive components—such as superconducting coils and electronics [5]. It is therefore important to examine and quantify the influence of activated water on the reactor environment.

Current knowledge of the reaction cross-sections relevant to water activation remains limited. Cross-section data often differ significantly between nuclear data libraries and, in many cases, carry large uncertainties [6]. Experiments that analyse activated water products could contribute to reducing these uncertainties.

In order to improve the understanding and modelling of water-activation processes and to directly support ITER [8, 9], a closed water-activation loop named KATANA was commissioned in late 2023 at the (TRIGA: Training, Research, Isotope production, General Atomics) Mark II research reactor of the Jožef Stefan Institute (JSI) in Slovenia [10]. The facility can serve as a stable source of both γ rays and neutrons. Owing to its high and stable flow rate (up to $0.7\,l\cdot s^{-1}$), high activities of ^{16}N, ^{17}N and ^{19}O can be achieved, which helps to minimise experimental uncertainties [11]. Preliminary analyses indicate that KATANA is suitable for experimental validation of fluid-activation codes relevant to ITER, DEMO [12, 13] and other future fusion devices [11, 14, 15].

Although some water-activation simulations for ITER [16] and DEMO [17] have been performed. Activated water remains poorly understood as a radiation source because of the lack of experimental data, in particular under fusion-relevant conditions. Two leading water-activation experiments using 14 MeV D–T neutron generators, the Frascati Neutron Generator (Italy) [18] and the Fusion Neutronic Source (Japan) [19, 20], have provided valuable data that support fusion research and ITER-related studies [21–25]. However, these experiments are no longer operational. Limitations of past facilities include relatively small irradiated volumes and limited availability. In this context, the KATANA water-activation loop fills an important research gap by enabling extended investigations of water activation.

The neutron spectra of fission and fusion reactors differ significantly. Prompt fission neutrons are emitted with a Maxwellian-like distribution peaking below 1 MeV and with an average energy around 2 MeV [26, 27], whereas D–T fusion produces almost monoenergetic neutrons with an energy near 14.1 MeV [28]. Figure 1 shows the prompt fission neutron spectrum of ^{235}U, the D–T neutron spectrum, and cross-sections of key water-activation reactions. The $^{18}O(n,\gamma)^{19}O$ reaction occurs primarily with thermal neutrons, whereas $^{16}O(n,p)^{16}N$ and $^{17}O(n,p)^{17}N$ are threshold reactions with energy thresholds of about 10 MeV and 8 MeV, respectively. Therefore, water activation is more prevalent in fusion environments with high-energy neutrons. Since only about 0.3% of prompt ^{235}U fission neutrons exceed 9 MeV and only about 0.1% exceed 10.5 MeV, the contribution of water activation in fission reactors is limited [4]. Nevertheless, the same water-activation products can be produced in both fusion and fission environments. Furthermore, water activation in fusion reactors is estimated to be several orders of magnitude larger than in fission reactors of comparable power [4]. Although the absolute specific activity of water is not critical for validation experiments—because the neutron transport equation is linear and results can be extrapolated—fission reactors can still be used for fusion-relevant experiments [29, 30].

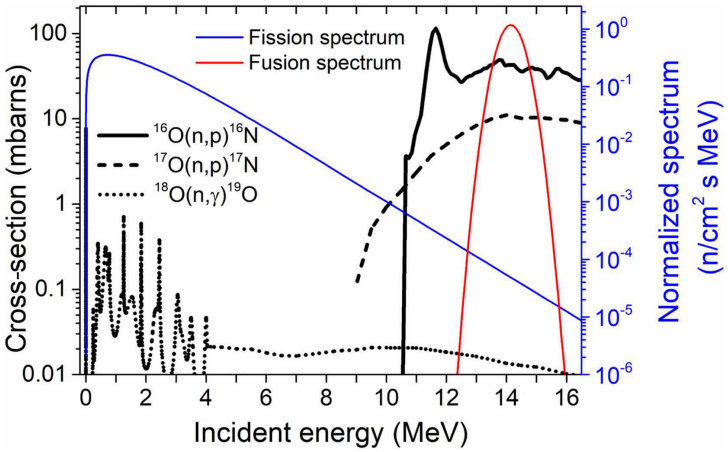

Figure 1. ^{235}U prompt fission neutron spectrum (blue) [27] and D–T fusion neutron spectrum (red), both normalised to a neutron flux of 1 n · cm^{-2} · s^{-1} per MeV. Cross-sections for water-activation reactions (black) are based on the FENDL-3.2b data library [31]. Reproduced with permission from [10]. CC BY-NC-ND 4.0.

This work investigates the feasibility of detecting and quantifying neutrons emitted in the decay of ^{17}N using the neutron activation method [32]. Additionally, this method is proposed to estimate the KATANA neutron emission rate and to evaluate the neutron fluence at selected sample locations.

The outcomes of this study may broaden the application of the neutron activation method to detect neutrons emitted by activation products in water—an approach, to the authors' knowledge, not previously applied to this problem. The results will support the experimental characterisation of the newly commissioned KATANA water-activation loop, assist validation of fluid–activation codes, and help reduce uncertainties in water-activation experiments.

This paper is organised as follows. Section 2 describes the KATANA water-activation loop, presents the pre-analysis used to select suitable neutron activation monitors, and summarises the experimental conditions. Section 3 describes the proposed methodology and details the MCNP simulations. Section 4 presents gamma-spectrometry measurements for analysed samples, the determined activities of produced nuclides, and assessed experimental reaction rates. The section also includes MCNP predictions of the neutron-fluence energy spectrum and calculated reaction rates, leading to the derived neutron emission rate of the KATANA water-activation loop and estimated neutron fluence at sample positions. Section 5 summarises the main conclusions of this work.

2. Experiments at KATANA water-activation loop

The JSI operates a TRIGA Mark II research reactor. The reactor is a 250 kW light-water pool-type facility cooled by natural convection [33]. A useful feature for simulating fusion devices is that the TRIGA reactor can simulate pulse operation by reaching peak powers of up to 1 GW for several milliseconds [34, 35].

The reactor includes several irradiation channels; in particular, the radial piercing port (RPP) passes through the graphite reflector and reaches the reactor core. An analysis has shown that the RPP is the most suitable location for implementing an irradiation facility that utilises a closed-water-activation loop [36].

The KATANA water-activation loop is shown in figure 2. It consists of three parts: the inner irradiation part, where water activation occurs; transport tubes that convey activated water from the RPP to the outer observation section; and the outer observation part (referred to hereafter as the KATANA snail) - the final piece of the loop, designed to accumulate the activated water in a defined region where detectors can be placed to measure γ rays and neutrons.

2.1. Preliminary analysis for selection of neutron-activation monitors

In order to select the most suitable neutron activation monitors for irradiation experiments at KATANA, a detailed pre-analysis was performed. A set of FISPACT-II [38] simulations was carried out for selected materials: Au, Co, Cr, In, Mn, Mo, Nb, Ni, Sc and Ta. These materials were considered for irradiation in a given neutron flux for 3 h, 8 h and 12 h. The neutron spectra used as input for the FISPACT-II calculations were based on neutron emissions resulting from the decay of ^{17}N; these emissions occur at the

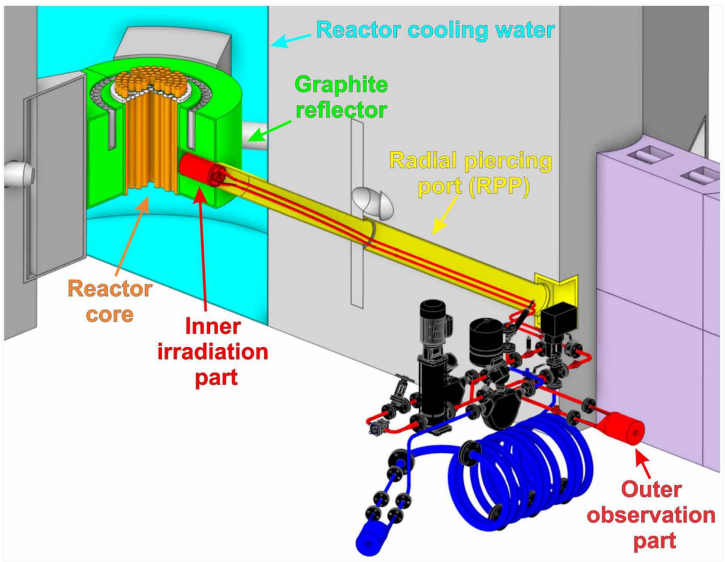

Figure 2. Schematic drawing of the KATANA water-activation loop, showing its three main components: the inner irradiation part, the transport tubes (partly located in the RPP), and the outer observation part (KATANA snail) for placement of γ and neutron detectors. Adapted with permission from [37].

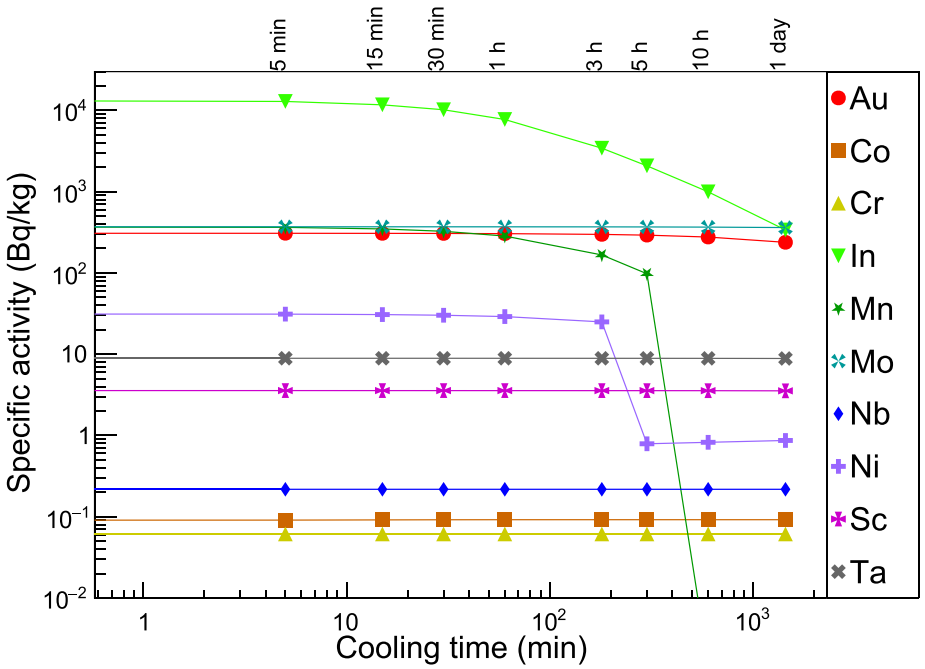

Figure 3. Calculated specific activity of selected neutron activation monitors at selected cooling intervals following 8 h of irradiation.

three discrete energies listed in table 1. For a coolant flow rate of $0.51 \cdot s^{-1}$, the total neutron emission rate from ^{17}N decay was estimated as $1.11 \times 10^4 n \cdot s^{-1}$ [39]. All simulations employed the TENDL-2017 nuclear data library [40].

Figure 3 presents the FISPACT-calculated specific activities for the considered neutron activation monitors at selected cooling intervals following an 8 h irradiation. The indium activation sample exhibits the highest specific activity after irradiation. In addition to predicted activity, other selection criteria were applied. Activation monitors had to be small enough to fit inside the KATANA snail (where the neutron flux is approximately 30% higher than outside the snail [41]), or sufficiently massive so that irradiation outside the snail would yield measurable activity. The nuclides produced in the candidate samples should emit gamma rays with well-defined energies and sufficient intensities for gamma-spectrometry detection, and should have half-lives long enough to permit reliable measurement.

Table 2. Properties of the samples selected for irradiation at the KATANA water-activation loop during the experimental campaign.

Sample name	Mass (g)	Thickness (mm)	Diameter (mm)
Au-1	9.9883	2.02	18.25
Au-2	9.9989	1.99	18.11
Au-11	0.4942	0.11	17.81
Au-12	0.4698	0.10	17.87
Au-13	0.4919	0.10	17.92
Au-14	0.5025	0.10	18.07
Au-15	0.4992	0.10	18.02
Au-16	0.4561	0.09	18.07
In-1	99.8603	4.73	63.59
In-2	100.2736	4.41	63.31
In-3	99.3851	4.38	63.23
In-5	99.6281	4.44	62.84
In-6	98.3570	4.46	63.29
Ni-6	92.2603	3.64	60.36
Ni-8	103.6357	4.09	60.11

Considering these criteria, three neutron activation monitors were selected for the experimental campaign: indium, gold and nickel.

For the indium samples, neutron irradiation is expected to produce two metastable nuclides: ^{115m}In and ^{116m}In. Both emit well-defined gamma rays with high intensities and have half-lives sufficient for reliable detection. However, the contribution from ^{116m}In is not useful for neutron-fluence estimation because the $^{115}\mathrm{In}(n,\gamma)^{116m}\mathrm{In}$ cross-section exhibits numerous resonances, which complicate fluence determination. By contrast, ^{115m}In is suitable for fluence estimation and will be examined in the measured gamma spectra.

In the case of gold, the likely activation products are ^{197m}Au and ^{198}Au. The isomer ^{197m}Au is produced in a reaction with a relatively smooth cross-section but has a very short half-life (7.73 s) and may therefore be unobservable in a gamma energy spectrum. The nuclide ^{198}Au has a longer half-life and emits an intense gamma line; however, the $^{197}\mathrm{Au}(n,\gamma)^{198}\mathrm{Au}$ reaction cross-section exhibits a resonance structure. Consequently, gold is more suitable as an indicator of neutron presence than as a precise fluence monitor.

For nickel, production of ^{58}Co is expected. This radionuclide emits a gamma ray with a high branching ratio (99.45%) and is produced via reactions with relatively smooth (non-resonant) cross-sections, making ^{58}Co a suitable choice for neutron-fluence determination from measured gamma spectrum.

Table 2 summarises the properties of the samples selected for irradiation at the KATANA water-activation loop during the experimental campaign.

2.2. Experimental setup

The experimental campaign at the KATANA water-activation loop lasted six days. The irradiation time was increased progressively from 2 h to 4 h, 6 h and 7 h, reaching 20 h on the final day. During all irradiation days the reactor operated at a constant power of 250 kW. The water flow rate was $0.681\,\mathrm{l}\cdot\mathrm{s}^{-1}$ on days 1, 2, 4 and 5, and $0.690\,\mathrm{l}\cdot\mathrm{s}^{-1}$ on days 3 and 6. Samples small enough to fit inside the KATANA snail were placed within it; larger samples were positioned outside. Figure 4 shows the two irradiation geometries used for samples of different sizes. Detailed information on sample placement, irradiation, cooling and gamma-spectrometry measurement times is given in table 3.

Samples In-5 and In-6 were irradiated under a cadmium cover to suppress the contribution of thermal neutrons [42, 43]. This shielding reduced the production of ^{116m}In, which is not useful for fluence determination, and decreased the Compton background, thereby improving the visibility of the ^{115m}In peak.

After irradiation, samples were measured on JSI's ORTEC HPGe coaxial detector (relative efficiency 40%, energy resolution 1.85 keV at 1332 keV). Efficiency calibration was performed with ANGLE5 software [44, 45] using the known efficiency curve of the calibration source. A dedicated efficiency curve was determined for each analysed sample. Figure 5 presents an example of the resulting energy–efficiency calibration curve for an In-6 sample.

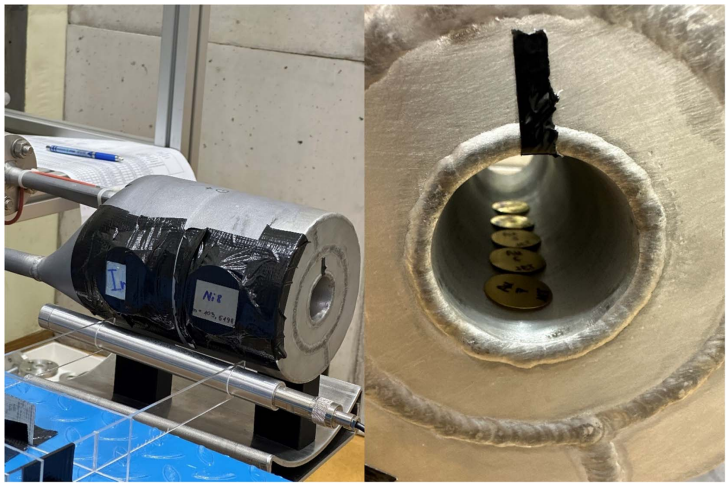

Figure 4. Irradiation geometries. Left: larger samples positioned outside the KATANA snail. Right: smaller samples placed inside the snail.

Table 3. Sample irradiation strategy at the KATANA water-activation loop, listing campaign day, irradiation time, sample name, irradiation location, cooling time, and gamma-spectrometry measurement duration. Sample Ni-8 was positioned outside the KATANA snail and irradiated at that location from days 3–6; gamma-spectrometry measurement was performed after day 6.

Campaign day	Irradiation time (s)	Sample name	Irradiation location	Cooling time (s)	Counting time (s)
1st	7177	Au-11 and Au-12	Inside the snail	4	376
		In-1	Outside the snail	1425	60 887
		Ni-6	Outside the snail	62 609	18 705
2nd	14 365	Au-13 – Au-16	Inside the snail	137	14 524
		In-2	Outside the snail	14 979	52 689
3rd	21 631	Au-1 and Au-2	Inside the snail	24	62 573
		In-3	Outside the snail	297	83 580
		Ni-8	Outside the snail	—	—
4th	21 600	Ni-8	Outside the snail	—	—
5th	25 201	In-5	Outside the snail	250	235 821
		Ni-8	Outside the snail	—	—
6th	71 380	In-6	Outside the snail	266	130 079
		Ni-8	Outside the snail	330 049	777 378

3. Methodology and modelling

Gamma-spectrometry measurements on an HPGe detector enable the determination of the gamma-energy spectrum emitted by an irradiated sample. After an energy-efficiency calibration, the activities of nuclides produced in the sample can be determined. The activity of a nuclide is derived using the relation presented in equation (1) [46], where N_{net} is the net peak area of the selected γ peak, $\varepsilon_{\mathrm{eff}}(E)$ is the full-energy peak efficiency at energy E, y is the emission probability (branching ratio) of the selected γ line, t_{l} is the live time of the acquisition (s), K_{c} is the decay-correction factor for the cooling period (from the end of irradiation to the start of acquisition) and K_{m} is the decay-correction factor for the nuclide decay during the measurement,

$$A_0 = \frac{N_{\mathrm{net}}}{\varepsilon_{\mathrm{eff}}(E)\, y\, t_{\mathrm{l}}\, K_{\mathrm{c}}\, K_{\mathrm{m}}}. \tag{1}$$

The cooling-time correction factor is shown in equation (2), where t_{c} is the elapsed time between the end of irradiation and the start of the gamma energy spectrum acquisition (s), and $T_{1/2}$ is the nuclide half-life (s),

$$K_{\mathrm{c}} = \exp(-\lambda t_{\mathrm{c}}) \quad \text{with} \quad \lambda = \frac{\ln 2}{T_{1/2}}. \tag{2}$$

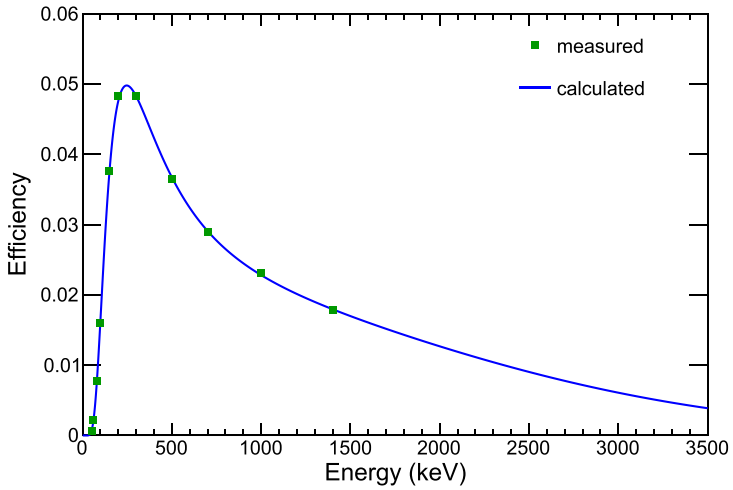

Figure 5. Energy-efficiency calibration curve obtained with ANGLE5 software for an In-6 sample.

The correction factor that accounts for decay during counting is expressed by equation (3), where t_m is the clock time of the measurement (s),

$$K_m = \frac{1}{\lambda t_m}\left(1 - \exp\left(-\lambda t_m\right)\right). \tag{3}$$

Some samples used in this work were relatively thick (4.38–4.73 mm). To account for γ self-absorption, a self-absorption correction factor F_{abs} was applied [47, 48]. Using mass attenuation coefficients from [49], the calculation of F_{abs} is given in equation (4), where μ/ρ is the mass attenuation coefficient ($cm^2 \cdot g^{-1}$), m is the sample mass (g), and S is the sample surface area (cm^2),

$$F_{abs} = \frac{(\mu/\rho)\, m}{S\left[1 - \exp\left(-\dfrac{(\mu/\rho)\, m}{S}\right)\right]}. \tag{4}$$

The activity corrected for γ self-absorption is expressed by equation (5),

$$A = A_0 \cdot F_{abs}. \tag{5}$$

From the measured activity of the activation product, the experimental reaction rate RR_{exp} can be derived using equation (6) [50], where A is the activity of the produced nuclide (Bq), M is the atomic mass of the target nucleus ($g{\cdot}mol^{-1}$), m is the mass of the irradiated sample (g), f_i is the isotopic abundance (fraction) of the target nuclide, N_A is Avogadro's constant (mol^{-1}), λ is the decay constant (s^{-1}), and t_{irr} is the irradiation time (s),

$$RR_{exp} = \frac{AM}{m f_i N_A \left(1 - \exp\left(-\lambda t_{irr}\right)\right)}. \tag{6}$$

3.1. MCNP modelling

In the neutronics model of the KATANA snail, the water inside is represented as a uniformly distributed neutron source with three discrete energies: 0.383 MeV (35%), 1.171 MeV (53%) and 1.700 MeV (7%). Activation samples were added to the geometry at the locations corresponding to their experimental placement. Figure 6 shows the CAD and neutronics representations of the snail with an indium sample attached.

Calculations were performed with MCNP6 [51] using the ENDF/B-VII.1 cross-section library [7]. Reaction rates per source neutron, RR_{MCNP}, were extracted with DE/DF cards using the $^{115}\mathrm{In}(n,n')^{115m}\mathrm{In}$ cross-section from TENDL-2019 (MF = 10, MT = 4).

MCNP reports reaction rates normalised per source neutron: each neutron sampled from the water-in-snail source is transported and its contribution to the reaction is recorded. Hence, the MCNP reaction rate represents the average contribution of a single source neutron, including neutrons that do not reach

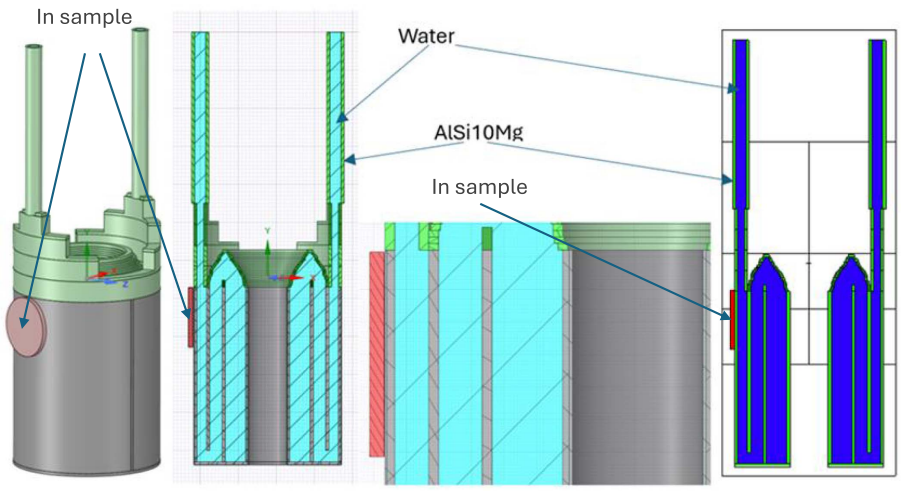

Figure 6. CAD and neutronics models of the KATANA snail with an indium activation sample placed at the location corresponding to the experiment.

the sample. Comparing the experimentally derived reaction rate RR_{exp} with the MCNP-calculated reaction rate per source neutron RR_{MCNP} yields the source strength (neutron emission rate—Q) as presented in equation (7),

$$Q = \frac{RR_{exp}}{RR_{MCNP}}. \tag{7}$$

Using the derived source strength Q and the MCNP-calculated neutron flux in the sample location per source neutron (tally F4 - φ), the neutron fluence at the sample location is expressed by equation (8). It is worth noting that in this methodology Q and φ are time-independent,

$$\Phi = Q \cdot t_{irr} \cdot \varphi. \tag{8}$$

4. Results

Gamma-spectrometry measurements for the gold samples (Au-11 and Au-12) were recorded with a short live time (376 s) to evaluate whether the short-lived isomer ^{197m}Au ($T_{1/2} \approx 7.73$ s) could be observed. Production of ^{197m}Au would be indicated by gamma lines at 130.2 keV, 201.6 keV and 279.0 keV. Despite the rapid acquisition, the nuclide was not detected, and no further analysis of the gamma energy spectrum for these samples was performed.

Gold activation products were also sought in spectra from Au-1, Au-2, Au-13, Au-14, Au-15, and Au-16. To increase the detection sensitivity, Au-1 and Au-2 were measured together. Likewise, Au-13 through Au-16 were also measured in a group. In both cases, ^{198}Au was detected, confirming neutron-induced activation of the gold samples.

The Ni-6 sample was irradiated for 2 h. The ^{58}Co peak expected at 810.76 keV, was not observed. Consequently, irradiation time for the nickel was increased: sample Ni-8 was irradiated over four campaign days (days 3–6) and its gamma energy spectrum was accumulated for an extended period (nearly nine days), but ^{58}Co remained unobserved.

The most promising results were obtained for the indium samples, and the following analysis focuses on these. Table 4 lists the detected gamma lines associated with ^{115m}In and ^{116m}In, together with the net peak-area uncertainties. In all gamma energy spectra measured for indium samples, the 336.24 keV line of ^{115m}In was observed. Representative gamma energy spectra for In-1, In-3 and In-6 are shown in figure 7. To improve readability, each observed peak is annotated with coloured markers that indicate the originating sample.

Sample In-1 (2 h irradiation) was counted about 0.4 h after irradiation for ≈17 h. The short cooling produced significant ^{116m}In contributions (strong lines at 416.90, 1097.28, 1293.56, 1507.59 and 2112.29 keV); net peak-area uncertainties for the most intense ^{116m}In lines were ≈3%–4%.

Sample In-2 (4 h irradiation) was measured after a ≈4 h cooling interval to suppress ^{116m}In (half-life ≈54 min). Although only two ^{116m}In lines remained, the extended cooling interval contributed to an

Table 4. Detected nuclides, gamma energy lines, emission probabilities and net peak-area uncertainties for the indium samples.

Sample name	Detected nuclide	Gamma energy line (keV)	Intensity (%)	Net peak area uncertainty (%)
In-1	^{115m}In	336.24	45.90	11.1
	^{116m}In	416.90	27.20	3.9
		1097.28	58.50	3.1
		1293.56	84.80	2.4
		1507.59	9.92	6.4
		2112.29	15.09	12.3
In-2	^{115m}In	336.24	45.90	26.1
	^{116m}In	1293.56	84.80	19.9
		1507.59	9.92	12.4
In-3	^{115m}In	336.24	45.90	10.7
	^{116m}In	416.90	27.20	3.7
		818.63	12.13	12.3
		1097.28	58.50	2.8
		1293.56	84.80	7.2
		1507.59	9.92	7.0
		2112.29	15.09	7.4
In-5	^{115m}In	336.24	45.90	23.1
	^{116m}In	1293.56	84.80	8.7
In-6	^{115m}In	336.24	45.90	6.6
	^{116m}In	416.90	27.20	19.5
		1097.28	58.50	10.2
		1293.56	84.80	6.7
		1507.59	9.92	6.8
		2112.29	15.09	20.6

increased net peak-area uncertainty for ^{115m}In (≈26%) and to a probable underestimation of the derived activity. Consequently, In-2 was excluded from further analysis to focus on higher-quality results.

For In-3 (6 h irradiation) counting began after a short cooling time (≈5 min) and continued for ≈24 h; both ^{115m}In and several ^{116m}In lines were observed.

In-5 was irradiated under a cadmium cover to suppress thermal-neutron activation of ^{116m}In. However, the very long counting period (≈65 h) allowed short-lived ^{116m}In to decay and bury its peaks in the background. Moreover, during such an extended measurement, the activity of ^{115m}In ($T_{1/2} \approx$ 4.4 h) decreases and the relative background contribution grows, degrading peak purity and increasing peak-area uncertainty to >20%. Consequently, the In-5 results are expected to underestimate the real ^{115m}In activity and were excluded from subsequent analysis.

In-6 (20 h irradiation, cadmium shield) was measured for ≈36 h. Some ^{116m}In lines were still present, but the long irradiation and shielding produced a relatively low net peak-area uncertainty for ^{115m}In (≈6.6%), yielding the most precise result for reaction-rate and fluence estimation.

4.1. Determination of the KATANA neutron emission rate

The activity of ^{115m}In was derived from equation (1). Gamma self-absorption was accounted for using equation (4), yielding the corrected activity in equation (5). Uncertainties were propagated using the law of propagation of uncertainty, adopting the uncertainty components recommended in [52]. The results are summarised in table 5.

The derived ^{115m}In activities increase with irradiation time. Using the corrected activities and equation (6), the experimental reaction rates RR_{exp} were assessed. MCNP reaction rates per source neutron RR_{MCNP} were obtained with DE/DF tallies. The neutron emission rate Q was derived from equation (7). Results are given in table 6.

4.2. Estimation of the neutron fluence at sample location

Using the MCNP model of the KATANA snail, the 709-group neutron flux density energy spectrum per unit lethargy per source neutron at each sample position was calculated. Results for the indium samples without and with a cadmium cover are shown in figure 8. The three prominent peaks visible in the

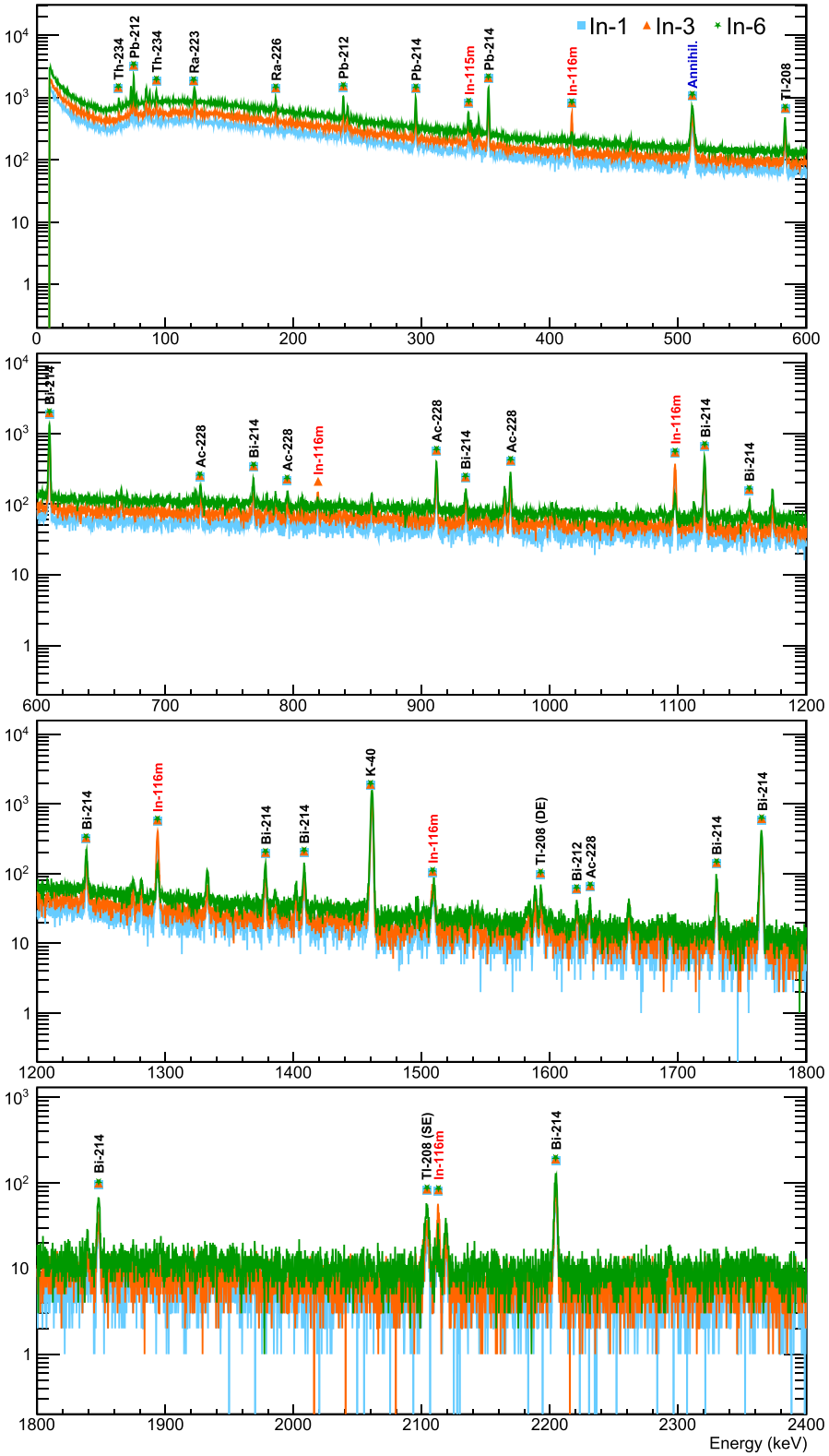

Figure 7. Representative gamma energy spectra for In-1, In-3 and In-6 samples. Peaks of interest are marked in red, background peaks in black and the annihilation peak in blue. Labels SE and DE next to nuclide names denote single- and double-escape peaks, respectively.

spectrum correspond to the three discrete neutron energies emitted in the decay of ^{17}N. Differences at low energies demonstrate that the cadmium cover effectively absorbs the thermal-neutron component and removes the lowest-energy portion of the spectrum.

Table 5. Gamma self-absorption factors and measured activities of ^{115m}In for the selected indium samples.

Sample name	Irradiation time (s)	Cooling time (s)	Counting time (s)	F_{abs}	Activity (Bq)
In-1	7177	1425	60 887	1.24 ± 0.04	1.33 ± 0.15
In-3	21 631	297	83 580	1.25 ± 0.04	2.27 ± 0.24
In-6	71 380	266	130 079	1.24 ± 0.04	3.34 ± 0.22

Table 6. Experimental and MCNP reaction rates for the indium samples, and derived neutron emission rates.

Sample name	RR_{exp} (s^{-1})	RR_{MCNP} (reactions per n)	Q (s^{-1})
In-1	$(10.00 \pm 1.12) \times 10^{-24}$	$(3.0155 \pm 0.0015) \times 10^{-29}$	$(3.33 \pm 0.37) \times 10^{5}$
In-3	$(7.52 \pm 0.81) \times 10^{-24}$	$(3.0313 \pm 0.0012) \times 10^{-29}$	$(2.48 \pm 0.27) \times 10^{5}$
In-6	$(7.04 \pm 0.47) \times 10^{-24}$	$(2.9000 \pm 0.0015) \times 10^{-29}$	$(2.43 \pm 0.16) \times 10^{5}$

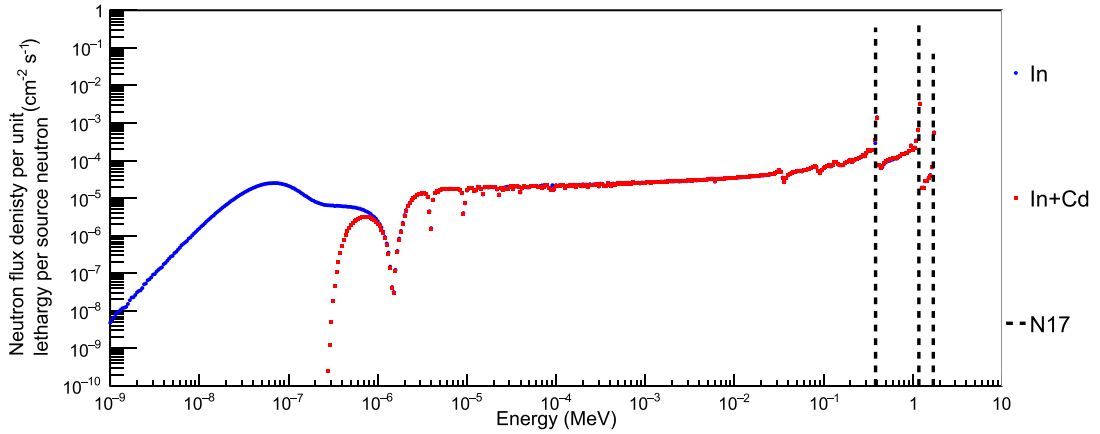

Figure 8. MCNP-calculated 709-group neutron flux density energy spectrum per unit lethargy per source neutron at the indium sample position, shown without (In) and with a cadmium cover (In+Cd). The labelled N17 peaks correspond to the three discrete neutron energies from ^{17}N decay.

Table 7. Neutron fluence and flux at the sample locations, derived for indium samples subjected to progressively longer irradiation times.

Sample name	Irradiation time (s)	Neutron fluence at the sample location (cm^{-2})	Neutron flux at the sample location ($cm^{-2}s^{-1}$)
In-1	7177	$(2.21 \pm 0.25) \times 10^{6}$	$(3.08 \pm 0.34) \times 10^{2}$
In-3	21 631	$(5.00 \pm 0.54) \times 10^{6}$	$(2.31 \pm 0.25) \times 10^{2}$
In-6	71 380	$(1.63 \pm 0.11) \times 10^{7}$	$(2.28 \pm 0.15) \times 10^{2}$

The neutron fluence at the sample location was then estimated from the assessed source strength Q and the MCNP-calculated neutron flux in the sample location per source neutron (see equation (8)). The resulting neutron fluence and flux at the sample location are listed in table 7.

A linear increase of neutron fluence with irradiation time is observed, as expected. The derived neutron flux at the sample location is relatively stable across the analysed samples. A comparison of the fluence and flux behaviour is presented in figure 9.

A linear fit to the neutron-fluence versus irradiation-time data was obtained by the least-squares method [53]. The slope of the best-fit line, which represents the neutron flux at the sample location, is

$$(228.76 \pm 5.44)\ \mathrm{cm}^{-2} \cdot \mathrm{s}^{-1}.$$

The flux estimates for In-3 and In-6 agree, within uncertainties, with the value determined from the linear fit to the neutron-fluence results. The flux derived from In-1 is slightly higher; this discrepancy may be attributed to the short irradiation time of In-1, making that measurement less reliable. The observed greater stability of results for longer irradiations suggests that extended irradiation times may improve the precision and reliability of activation measurements at the KATANA water-activation loop based on indium samples.

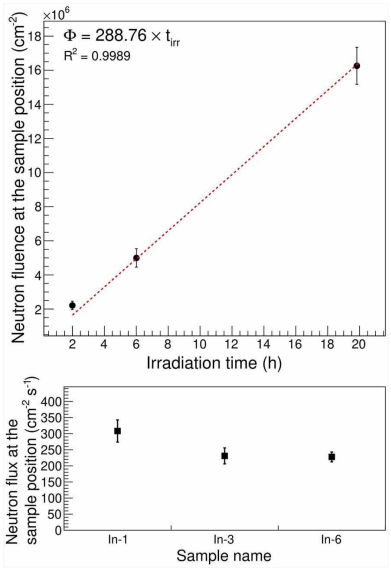

Figure 9. Comparison of fluence and flux behaviour for the analysed activation samples. Upper panel: neutron fluence at the sample location as a function of irradiation time; the least-squares linear fit is plotted; the fit equation and coefficient of determination (R^2) are reported in the inset. Lower panel: derived neutron fluxes at the sample location for the analysed samples.

5. Conclusions

The KATANA water-activation loop fills an important gap in experimental studies of water activation. It provides a stable source of both γ rays and neutrons (the latter produced by ^{17}N decay with well-defined energies), making it well suited for irradiation experiments. KATANA can directly support ITER-relevant research by enabling experimental validation of fluid-activation codes for the cooling systems of ITER, DEMO and other future fusion devices, and by helping to reduce experimental uncertainties in water-activation simulations.

A detailed pre-analysis with the FISPACT-II inventory code (see figure 3) identified indium, gold and nickel as the most suitable activation monitors for the assumed KATANA neutron spectrum. Subsequently, a series of irradiations was performed with these monitors.

Gamma energy spectra for gold samples revealed ^{198}Au, confirming the presence of neutrons originating from ^{17}N decay; the short-lived isomer ^{197m}Au was not observed despite rapid acquisition. Nickel activation (^{58}Co) was also not detected, likely because the ^{58}Ni$(n,p)^{58}$Co cross-section is relatively low ($\approx$20 mb at 1.7 MeV).

Indium proved to be the most effective monitor for ^{17}N neutrons at KATANA. The ^{115m}In 336.24 keV line was present in all indium spectra, and several ^{116m}In lines were identified (see figure 7). Irradiation, cooling and counting times were optimised to minimise uncertainty in the ^{115m}In activity; for two samples (In-5, In-6) a cadmium cover was used to suppress thermal neutrons. Gamma self-absorption corrections were applied when deriving activities.

The most precise result on ^{115m}In activity was obtained for sample In-6, owing to its long irradiation (20 h), an appropriate cooling schedule, extended counting and the use of a cadmium shield. Samples In-2 and In-5 yielded underestimated activities because of excessive cooling time (In-2) and excessively long counting (In-5); these samples were therefore excluded from the neutron-emission-rate determination. Final results are based on In-1, In-3 and In-6 samples.

From the measured ^{115m}In activities, experimental reaction rates were derived and compared with MCNP-calculated reaction rates per source neutron to obtain the KATANA neutron emission rate (see table 6). The three reliable sample estimates span $(2.43 \pm 0.16) \times 10^5\,\mathrm{n \cdot s^{-1}}$ to $(3.33 \pm 0.37) \times 10^5\,\mathrm{n \cdot s^{-1}}$; the values for In-3 and In-6 are in close agreement, while the estimate from In-1 is slightly higher, which likely reflects the lower reliability of the In-1 measurement because that sample was irradiated for the shortest time (2 h).

A method for estimating neutron fluence at selected sample locations was proposed (see equation (8)). The derived fluences increase with irradiation time, as expected (see table 7). A linear fit of fluence versus irradiation time (see figure 9) yields a neutron flux of $(228.76 \pm 5.44)\,\mathrm{cm}^{-2} \cdot \mathrm{s}^{-1}$, consistent, within uncertainties, with the fluxes derived from In-3 and In-6; the flux derived from In-1 is slightly larger, reflecting the lower reliability of that measurement.

The successful detection and quantification of ^{115m}In, produced by neutrons emitted in the decay of ^{17}N, demonstrates that the neutron activation method can be used to characterise neutrons from activated water at the KATANA water-activation loop. The results show how experimental conditions (irradiation/cooling times and cadmium shielding) can be tailored to improve sensitivity and precision for activation measurements at the KATANA water-activation loop.

Future work will characterise the neutron-fluence profile around the KATANA snail, further validate the proposed methodology, and provide experimental data for validation of fluid-activation codes for ITER, DEMO and other fusion devices. Results from KATANA are expected to reduce uncertainties in water-activation simulations and thereby contribute to improved safety assessments for fusion systems.

Acknowledgments

This scientific paper has been published as part of the international project co-financed by the Polish Ministry of Science and Higher Education within the programme called 'PMW'. This work has been carried out within the framework of the EUROfusion Consortium, funded by the European Union via the Euratom Research and Training Programme (Grant Agreement No 101052200 — EUROfusion). Views and opinions expressed are however those of the author(s) only and do not necessarily reflect those of the European Union or the European Commission. Neither the European Union nor the European Commission can be held responsible for them. We gratefully acknowledge Polish high-performance computing infrastructure PLGrid (HPC Center: ACK Cyfronet AGH) for providing computer facilities and support within computational Grant No. PLG/2024/017354.

Data availability statement

All data that support the findings of this study are included within the article (and any supplementary files).

Author contributions

J Wlodarczyk 0009-0004-8024-3439
Formal analysis (lead), Investigation (lead), Methodology (lead), Software (equal), Visualization (equal), Writing – original draft (lead)

B Bienkowska 0000-0003-1103-3441
Investigation (equal), Methodology (equal), Software (lead), Visualization (equal), Writing – review & editing (equal)

E Laszynska 0009-0009-4888-6369
Investigation (equal), Methodology (equal), Writing – review & editing (equal)

D Govekar
Writing – review & editing (supporting)

D Kotnik
Writing – review & editing (supporting)

I Lengar
Writing – review & editing (supporting)

X Litaudon 0000-0001-6973-9717
Writing – review & editing (supporting)

J Peric 0009-0003-9396-2574
Methodology (equal), Writing – review & editing (equal)

V Radulovic
Writing – review & editing (supporting)

L Snoj 0000-0003-3097-5928
Writing – review & editing (supporting)

R Villari 0000-0001-7972-1676
Writing – review & editing (supporting)

References

[1] Batistoni P *et al* 2017 WPJET3 NEXP report D21 – feasibility study of a water activation experiment at JET during DTE2 *Technical Report* (ENEA)
[2] Martinez A, Bayetti P, Bucalossi J, Chantant M, Missirlian M, Portafaix C and Samaille F 2012 upgrades of the tore supra water cooling system for the WEST project *2013. Proc. 27th Symp. On Fusion Technology* (*Fusion Engineering and Design SOFT-27*) (Belgium) vol 88 (Liège) pp 804–8
[3] Yang Q, Dang T, Ying D, Wang G and Loughlin M 2012 Activation analysis of coolant water in ITER blanket and divertor *Tenth Int. Symp. on Fusion Nuclear Technology (ISFNT-10)* (*Fusion Engineering and Design*) vol 87 pp 1310–4
[4] Žohar A and Snoj L 2019 On the dose fields due to activated cooling water in nuclear facilities *Prog. Nucl. Energy* **117** 103042
[5] Iida H, Plenteda R, Santoro R and Khripunov V 1997 Three-dimensional analysis of nuclear heating in the superconducting magnet system due to gamma-rays from /sup 16/n in the iter water cooling system of the shielding blanket *17th IEEE/NPSS Symp. Fusion Engineering (Cat. No.97CH36131)* vol 2 pp 837–40
[6] Žohar A, Lengar I and Snoj L 2020 Analysis of water activation in fusion and fission nuclear facilities *Fusion Eng. Des.* **160** 111828
[7] Brown D *et al* 2018 ENDF/B-VIII.0: the 8th major release of the nuclear reaction data library with CIELO-project cross sections, new standards and thermal scattering data *Nucl. Data Sheets* **148** 1–142
[8] Rebut P-H 1995 ITER: the first experimental fusion reactor *Fusion Eng. Des.* **30** 85–118
[9] Geng S 2022 An overview of the ITER project *J. Phys.: Conf. Ser.* **2386** 012012
[10] Kotnik D, Basavaraj A K, Snoj L and Lengar I 2023 Design optimization of the closed-water activation loop at the JSI irradiation facility *Fusion Eng. Des.* **193** 113632
[11] Kotnik D, Peric J, Govekar D, Snoj L and Lengar I 2025 KATANA - water activation facility at JSI TRIGA, Part I: final design and activity calculations *Nucl. Eng. Technol.* **57** 103233
[12] Bachmann C *et al* 2015 Initial DEMO tokamak design configuration studies *Proc. 28th Symp. Fusion Technology (SOFT-28)* (*Fusion Engineering and Design)* vol 98–99 pp 1423–6
[13] Coleman M, Zohm H, Bourdelle C, Maviglia F, Pearce A, Siccinio M, Spagnuolo A and Wiesen S 2025 Definition of an EU-DEMO design point robust to epistemic plasma physics uncertainties *Nucl. Fusion* **65** 036039
[14] Kotnik D, Peric J, Govekar D, Snoj L and Lengar I 2025 KATANA - water activation facility at JSI TRIGA, Part II: first experiments *Nucl. Eng. Technol.* **57** 103290
[15] Peric J, Kotnik D, Snoj L and Radulović V 2025 Neutron emission from water activation: experiments and modeling under fusion-relevant conditions at the katana facility *Fusion Eng. Des.* **216** 115052
[16] Ghani Z, Turner A, Mangham S, Naish J, Lis M, Packer L and Loughlin M 2015 Radiation levels in the iter tokamak complex during and after plasma operation *Proc. 28th Symp. Fusion Technology (SOFT-28)* (*Fusion Engineering and Design*) vol 96–97 pp 261–4
[17] Chiovaro P, Ciattaglia S, Cismondi F, Del Nevo A, Di Maio P, Federici G, Frittitta C, Moscato I, Spagnuolo G and Vallone E 2020 Investigation of the DEMO WCLL breeding blanket cooling water activation *Fusion Eng. Des.* **157** 111697
[18] Martone M, Angelone M and Pillon M 1994 The 14 MeV Frascati neutron generator *J. Nucl. Mater.* **212-215** 1661–4
[19] Uno Y *et al* 2001 Absolute measurement of D–T neutron flux with a monitor using activation of flowing water *Fusion Eng. Des.* **56–57** 895–8
[20] Konno C and Murata I 2014 Fusion Neutronics Source (FNS) Facility at Japan Atomic Energy Agency (available at: http://www-pub.iaea.org/MTCD/Publications/PDF/TE-1743-addCD_web.pdf)
[21] Ikeda Y, Uno Y, Maekawa F, Smith D L, Gomes I C, Ward R C and Filatenkov A A 1997 An investigation of the activation of water by D-T fusion neutrons and some implications for fusion reactor technology *Fusion Eng. Des.* **37** 107–50
[22] Andreoli F *et al* 2020 Comparison between measurement and calculations for a 14 MeV neutron water activation experiment *EPJ Web Conf.* **239** 21002
[23] Angelone M, Pillon M, Loreti S, Colangeli A, Mazzitelli G, Del Prete P, Villari R, Naish J, Nobs C and Packer L 2020 Measurement of delayed neutron emission from water activated by 14 MeV neutrons in a fw mock-up of ITER *Fusion Eng. Des.* **160** 111998
[24] Flammini D, Angelone M, Caiffi B, Colangeli A, Fonnesu N, Mariano G, Moro F and Villari R 2020 Pre-analysis of the WCLL breeding blanket mock-up neutronics experiment at the frascati neutron generator *Fusion Eng. Des.* **156** 111600
[25] Nobs C, Naish J, Packer L, Worrall R, Angelone M, Colangeli A, Loreti S, Pillon M and Villari R 2020 Computational evaluation of N-16 measurements for a 14 MeV neutron irradiation of an ITER first wall component with water circuit *Fusion Eng. Des.* **159** 111743
[26] Terrell J 1959 Fission neutron spectra and nuclear temperatures *Phys. Rev.* **113** 527–41
[27] Trkov A and Capote R 2015 Evaluation of the prompt fission neutron spectrum of thermal-neutron induced fission in U-235 *Phys. Proc.* **64** 48–54
[28] Kikuchi M, Lackner K and Tran M Q 2012 *Fusion Physics* (International Atomic Energy Agency) (available at: https://www-pub.iaea.org/MTCD/Publications/PDF/Pub1562_web.pdf)
[29] Bell G I and Glasstone S 1970 Nuclear reactor theory Van Nostrand Reinhold Company (available at: www.osti.gov/biblio/4074688)
[30] Prinja A and Larsen E 2010 *General Principles of Neutron Transport* (Springer) (https://doi.org/10.1007/978-0-387-98149-9_5)
[31] Schnabel G *et al* 2024 FENDL: a library for fusion research and applications *Nucl. Data Sheets* **193** 1–78
[32] Greenberg R R, Bode P and De Nadai Fernandes E A 2011 Neutron activation analysis: a primary method of measurement *Spectrochim. Acta B At. Spectrosc.* **66** 193–241
[33] Štancar Ž *et al* 2017 Reaction rate distribution experiments at the Slovenian JSI Triga Mark II research reactor *International Handbook of Evaluated Reactor Physics Benchmark Experiments* (OECD Nuclear Energy Agency) p 250

[34] Mele I, Ravnik M and Trkov A 1994 TRIGA mark II benchmark experiment, part II: pulse operation *Nucl. Technol.* **105** 52–58
[35] Švajger I, Čalič D, Pungerčič A, Trkov A and Snoj L 2024 Evaluation of reactor pulse experiments *Nucl. Eng. Technol.* **56** 1165–203
[36] Žohar A, Pungerčič A, Ambrožič K, Radulović V, Jazbec A, Rupnik S, Lengar I and Snoj L 2020 Conceptual design of irradiation facility with 6 MeV and 7 MeV gamma rays at the JSI TRIGA mark II research reactor *EPJ Web Conf.* **225** 04014
[37] Jožef Stefan Institute 2024 Katana JSI water activation loop (available at: https://katana.ijs.si/) (Accessed 03 October 2025)
[38] Sublet J-C, Eastwood J, Morgan J, Gilbert M, Fleming M and Arter W 2017 FISPACT-II: an advanced simulation system for activation, transmutation and material modelling *Nucl. Data Sheets* **139** 77–137
[39] de Pietri M *et al* 2023 Implementation of FLUNED for the JSI TRIGA water cooling loop and simulation of the radiation of complex water circuits *Deliverable Report EFDA_D_2R8GPX EUROfusion Deliverable Report* (CIEMAT)
[40] Koning A, Rochman D, Sublet J-C, Dzysiuk N, Fleming M and van der Marck S 2019 TENDL: complete nuclear data library for innovative nuclear science and technology *Nucl. Data Sheets* **155** 1–55
[41] Peric J, Kotnik D, Govekar D, Snoj L, Vykydalc Z, Pietri M D and Radulović V 2025 Neutron detector calibration for the katana facility: experimental and computational validation of water activation neutron emission *Fusion Eng. Des.* (https://doi.org/10.2139/ssrn.6172220)
[42] Moyer B J, Peters B and Schmidt F H 1946 Absorption of slow neutrons by Cd^{113} *Phys. Rev.* **69** 666
[43] Mughabghab S F 2018 *Atlas of Neutron Resonances* 6th edn (Elsevier)
[44] Jovanovic S, Dlabac A and Mihaljevic N 2010 *ANGLE v2.1—New version of the computer code for semiconductor detector gamma-efficiency calculations* (https://doi.org/10.1016/j.nima.2010.02.058)
[45] ANGLE Software *ANGLE5* user guide 2025 (available at: https://www.angle.me/downloads.html)(Accessed 03 October 2025)
[46] Canberra Industries 2004 Genie 2000 Spectroscopy Software Customization Tools (available at: http://depni.sinp.msu.ru/~hatta/canberra/Genie%202000%20Customization%20Tools%20Manual.pdf)
[47] Nakajima K, Akai M, Yamamoto T, Hashimoto M and and T S 1994 Measurements and analyses of the ratio of 238U captures to 235U fission in low-enriched UO2 tight lattices *J. Nucl. Sci. Technol.* **31** 1160–70
[48] Nakajima K, Akai M and and T S 1994 Measurements of the modified conversion ratio by gamma-ray spectrometry of fuel rods for water-moderated UO2 cores *Nucl. Sci. Eng.* **116** 138–46
[49] Hubbell J H and Seltzer S M 2004 *Tables of X-Ray Mass Attenuation Coefficients and Mass Energy-Absorption Coefficients* National Institute of Standards and Technology (https://doi.org/10.18434/T4D01F)
[50] Laszynska E, Jednorog S, Ziolkowski A, Gierlik M and Rzadkiewicz J 2015 Determination of the emission rate for the 14 MeV neutron generator with the use of radio-yttrium *Nukleonika* **60** 319–22
[51] Goorley J T *et al* (Los Alamos National Laboratory) 2013 Initial MCNP6 Release Overview - MCNP6 Version 1.0. (available at: https://scispace.com/pdf/initial-mcnp6-release-overview-mcnp6-version-1-0-2oyelp09z4.pdf)
[52] Santos A D, Tsiboulia A M, Snoj L, Radulovic V, Stancar Z, Szatmary Z, Blaise P D, Bess J D, Marshall M and Briggs J B 2017 *International reactor physics experiments evaluation project (IRPhEP) guide to the expression of uncertainty* (Nuclear Energy Agency (NEA)) (available at: https://www.oecd-nea.org/upload/docs/application/pdf/2021-07/uncguide_irphep.pdf)
[53] Bjorck Å 1996 *Numerical Methods for Least Squares Problems* (Society for Industrial and Applied Mathematics) (https://doi.org/10.1137/1.9781611971484)